Combined Effects of Hall Currents and Rotation on MHD Mixed Convection Oscillating Flow in a Rotating Vertical Channel

S. K. Guchhait
Department of Applied Mathematics Vidyasagar University
Midnapore 721 102, India

S.Das
Department of Mathematics
University of GourBanga
Malda 732 103, India

R.N.Jana
Department of AppliedMathematics
Vidyasagar University
Midnapore 721 102, India

ABSTRACT
Combined effects of Hall currents and rotation on MHD mixed convection in a rotating vertical channel have been studied. The governing equations are solved analytically in closed form. The effects of the various parameters on the velocity field, shear stresses, temperature field and the rate of heat transfer in terms of their amplitudes and tangent of phases are presented graphically. It is observed that the primary velocity decreases while the magnitude of the secondary velocity increases with an increase in Hall parameter parameter. It is also observed that both the primary velocity and the magnitude of the secondary velocity decrease with an increase in radiation parameter. Further, it is seen that the amplitudes of rate of heat transfer at the plates increases with an increase in either Prandtl number or radiation parameter or frequency parameter.

Keywords: Hall Currents, mixed convection, magnetic parameter, rotation parameter, radiation parameter, Prandtl number, Grashof number and oscillatory plate temperature.

1. INTRODUCTION

In many of the studies carried on hydromagnetic flow of a radiating fluid inside a vertical channel or over the vertical plate the effect of Hall currents in an unsteady state was often neglected. From practical point of view the effect of Hall currents cannot be ignored because of its important in many flow problems. The combined effects of Hall currents and radiation on the magnetohydrodynamic flows continue to attract the attention of engineering science and applied mathematics researchers owing to extensive applications of such flows in the context of ionized aerodynamics, nuclear energy systems control, improved designs in aerospace MHD energy systems, manufacture of advanced aerospace materials etc. Both analytical and computational solutions have been presented to a wide spectrum of problems. Free and forced convective flow of an electrically conducting fluid through the vertical channel under the influence of magnetic field occurs in many industrial and technical applications which include plasma studies, the boundary layer control in aerodynamics, petroleum industries, MHD power generators, cooling of nuclear reactors, and crystal growth. Helliwell and Mosa [1] reported on thermal radiation effects in buoyancy-driven hydromagnetic flow in a horizontal .

In the present paper, we have studied the combined effects of Hall currents and rotation on MHD mixed convection oscillating flow in a rotating vertical channel. It is seen that the primary velocity u_1 decreases with an increase in either magnetic parameter M^2 or radiation parameter R or Hall parameter m or rotation parameter K^2 or $n\tau$ and it increases with an increase in either Grashof number Gr or Prandtl number Pr or n. It is also seen that the magnitude of the secondary velocity v_1 increases with an increase in either Hall parameter m or Grashof number Gr or Prandtl number Pr

channel flow with an axial temperature gradient in the presence of Joule and viscous heating. The Hall currents and surface temperature oscillation effects on natural convection magnetohydrodynamic heat-generating flow were considered by Takhar and Ram [2]. Alagoa et al. [3] studied

magnetohydrodynamic optically-transparent free-convection flow, with radiative heat transfer in porous media with time-dependent suction using an asymptotic approximation, showing that thermal radiation exerts a significant effect on the flow dynamics. The magnetohydrodynamic free convection heat and mass transfer of a heat generating fluid past an impulsively started infinite vertical porous plate with Hall current and radiation absorption was studied by Kinyanjui [4]. The thermal radiation interaction with unsteady MHD flow past a vertical porous plate immersed in a porous medium was investigated by Samad and Rahman [5]. Chaudhary and Jain [6] studied the behaviours of unsteady hydromagnetic flow of a viscoelastic fluid from a radiative vertical porous plate. The effects of thermal radiation and Hall currents on magnetohydrodynamic free-convective flow and mass transfer over a stretching sheet with variable viscosity in the presence of heat generation/absorption were investigated Shit and Haldar [7]. Israel-Cookey [8] studied the MHD oscillatory Couette flow of a radiating viscous fluid in a porous medium with periodic wall temperature. An analytical model of MHD mixed convective radiating fluid with viscous dissipative heat has been presented by Ahmed and Batin [9]. The effects of thermal radiation, Hall currents, Soret and Dufour on MHD flow by mixed convection over a vertical surface in porous media where described by Shateyi [10]. Singh and Pathak [11] has conducted an analysis of an oscillatory rotating MHD Poiseuille flow with injection/suction and Hall Currents. Aurangzaib and Sharidan Shafie [12] have studied the effects of Soret and Dufour on unsteady MHD flow by mixed convection over a vertical surface in porous media with internal heat generation, chemical reaction and Hall currents. The exact solution of MHD mixed convection periodic flow in a rotating vertical channel with heat radiation has been presented by Singh [13]. Singh and Pathak [14] have discussed the effect of rotation and Hall currents on mixed convection MHD flow through a porous medium in a vertical channel in the presence of thermal radiation

and it decreases with an increase in either radiation parameter R or phase angle $n\tau$ or magnetic parameter M^2 or rotation parameter K^2 or frequency parameter n.

2. FORMULATION OF THE PROBLEM AND ITS SOLUTIONS

Consider an unsteady MHD flow of a viscous incompressible electrically conducting radiative fluid in a vertical channel on taking Hall currents into account. Choose a Cartesian co-ordinates system with x-axis in the direction of the flow, the z-axis is normal to the plate and the y-axis is perpendicular to zx-plane (see Fig.1). The channel and the fluid rotate in unision with the uniform angular velocity Ω about z-axis. The temperature of the plate at $(z = -h)$ is raised or lowered to $T_2 + (T_1 - T_2)\cos\omega t$ and the constant temperature T_2 is maintained at the plate $(z = h)$. A uniform transverse magnetic field B_0 acts along the z-axis and the plates are electrically non-conducting. The horizontal homogeneity of the problem shows that the physical quantities are function of z and t only, t being the time variable. The equation of continuity $\nabla \cdot \vec{q} = 0$ gives $w = 0$ where $\vec{q} \equiv (u, v, 0)$, u, v and 0 being the velocity components along the coordinates axes. The fluid is considered to be gray, absorbing emitting radiation but non-scattering medium.

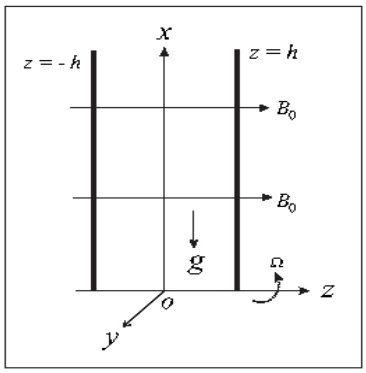

Figure 1: Geometry of the problem

The Boussinesq approximation is assumed to hold and for the evaluation of the gravitational body force, the density is assumed to be dependent on the temperature according to the equation of state

$$\rho = \rho_0[1 - \beta(T - T_2)], \tag{1}$$

where T is the fluid temperature, ρ the fluid density, β the coefficient of thermal expansion and ρ_0 the reference fluid density.

Using Boussinesq approximation, the momentum equations of motion along x and y-directions are

$$\frac{\partial u}{\partial t} - 2\Omega v = -\frac{1}{\rho}\frac{\partial p}{\partial x} + \nu\frac{\partial^2 u}{\partial z^2} + g\beta(T - T_2) + \frac{B_0}{\rho} j_y, \tag{2}$$

$$\frac{\partial v}{\partial t} + 2\Omega u = \nu\frac{\partial^2 v}{\partial z^2} - \frac{B_0}{\rho} j_x, \tag{3}$$

where ρ, ν and p are respectively the fluid density, the kinematic coefficient of viscosity and the modified fluid pressure.

Neglecting ion-slip and thermoelectric effects, the generalised Ohm's law for partially ionized gas is (see Cowling[15])

$$\vec{j} + \frac{\omega_e \tau_e}{B_0}(\vec{j} \times \vec{B}) = \sigma(\vec{E} + \vec{q} \times \vec{B}), \tag{4}$$

where $\vec{B}$, $\vec{E}$, $\vec{q}$, $\vec{j}$, σ, ω_e and τ_e are respectively, the magnetic field vector, the electric field vector, the fluid velocity vector, the current density vector, the conductivity of the fluid, the cyclotron frequency and the electron collision time.

We shall assume that the magnetic Reynolds number for the flow is small so that the induced magnetic field can be neglected. This assumption is justified since the magnetic Reynolds number is generally very small for partially ionized gases. The solenoidal relation $\nabla.\vec{B} = 0$ for the magnetic field gives $B_z = B_0 =$ constant everywhere in the fluid where $\vec{B} \equiv (B_x, B_y, B_z)$. The equation of the conservation of the charge $\nabla \cdot \vec{j} = 0$ gives $j_z =$ constant. This constant is zero since $j_z = 0$ at the plate which is electrically non-conducting. Thus $j_z = 0$ everywhere in the flow field. Since the induced magnetic field is neglected, the Maxwell's equation $\nabla \times \vec{E} = -\frac{\partial \vec{B}}{\partial t}$ becomes $\nabla \times \vec{E} = 0$ which gives $\frac{\partial E_x}{\partial z} = 0$ and $\frac{\partial E_y}{\partial z} = 0$. This implies that $E_x =$ constant and $E_y =$ constant everywhere in the flow.

In view of the above assumption, equation (4) gives, on taking $E_x = 0$ and $E_y = 0$.

$$j_x + m j_y = \sigma v B_0, \tag{5}$$

$$j_y - m j_x = -\sigma u B_0, \tag{6}$$

where $m = \omega_e \tau_e$ is the Hall parameter.

Solving for j_x and j_y, we get

$$j_x = \frac{\sigma B_0}{1 + m^2}(mu + v), \tag{7}$$

$$j_y = \frac{\sigma B_0}{1 + m^2}(mv - u). \tag{8}$$

On the use of equations (7) and (8), the equations (2) and (3) become

$$\frac{\partial u}{\partial t} - 2\Omega v = -\frac{1}{\rho}\frac{\partial p}{\partial x} + \nu\frac{\partial^2 u}{\partial z^2} + g\beta(T - T_2) + + \frac{\sigma B_0}{\rho(1 + m^2)}(mv - u), \tag{9}$$

$$\frac{\partial v}{\partial t} + 2\Omega u = \nu\frac{\partial^2 v}{\partial z^2} - \frac{\sigma B_0}{\rho(1 + m^2)}(v + mu). \tag{10}$$

The energy equation is

$$\rho c_p \frac{\partial T}{\partial t} = k\frac{\partial^2 T}{\partial z^2} - 16k^*\sigma^* T_2^3 (T - T_2), \tag{11}$$

where σ^* is the Stefan-Boltzman constant, k^* the spectral mean absorption coefficient of the medium, k the thermal conductivity and c_p the specific heat at constant pressure.

The boundary conditions for velocity and temperature distribution are

$$u = v = 0,\ T = T_2 + (T_1 - T_2)\cos\omega t \ \text{ at } \ z = -h,$$
$$u = v = 0,\ T = T_2 \ \text{ at } \ z = h. \tag{12}$$

Introducing non-dimensionless variables

$$(\eta, \xi) = (z, x)\frac{1}{h},\ (u_1, v_1) = (u, v)\frac{h}{\nu},\ \tau = \frac{\nu t}{h^2},\ \theta = \frac{T - T_2}{T_1 - T_2}, \tag{13}$$

equations (9), (10) and (11) become

$$\frac{\partial u_1}{\partial \tau} - 2K^2 v_1 = -\frac{\partial P}{\partial \xi} + \frac{\partial^2 u_1}{\partial \eta^2} - \frac{M^2}{1+m^2}(u_1 - m v_1) + Gr\theta, \quad (14)$$

$$\frac{\partial v_1}{\partial \tau} + 2K^2 u_1 = \frac{\partial^2 v_1}{\partial \eta^2} - \frac{M^2}{1+m^2}(v_1 + m u_1), \quad (15)$$

$$Pr\frac{\partial \theta}{\partial \tau} = \frac{\partial^2 \theta}{\partial \eta^2} - R\theta, \quad (16)$$

where $K^2 = \frac{\Omega h^2}{\nu}$ is the rotation parameter, $M^2 = \frac{\sigma B_0^2 h^2}{\rho \nu}$ the magnetic parameter, $Gr = \frac{g\beta(T_1 - T_2)h^2}{\nu^2}$ the Grashof number, $Pr = \frac{\rho c_p \nu}{k}$ the Prandtl number, $R = \frac{16k^*\sigma^* T_2^3 h^2}{k}$ the radiation parameter and $P = -\frac{h^2 p}{\rho \nu^2}$ the non-dimensional fluid pressure.

The boundary conditions (12) become

$$u_1 = v_1 = 0,\ \theta = \cos n\tau \ \text{ at } \ \eta = -1,$$
$$u_1 = v_1 = 0,\ \theta = 0 \ \text{ at } \ \eta = 1, \quad (17)$$

where $n = \frac{\omega h^2}{\nu}$ is the frequency parameter.

Combining the equations (14) and (15), we have

$$\frac{\partial F}{\partial \tau} = -\frac{\partial P}{\partial \xi} + \frac{\partial^2 F}{\partial \eta^2} - \left[2iK^2 + \frac{M^2(1+im)}{1+m^2}\right]F + Gr\theta, \quad (18)$$

where

$$F = u_1 + iv_1 \ \text{ and } \ i = \sqrt{-1}. \quad (19)$$

The corresponding boundary conditions for F and θ are

$$F = 0,\ \theta = \cos n\tau \ \text{ at } \ \eta = -1,$$
$$F = 0,\ \theta = 0 \ \text{ at } \ \eta = 1. \quad (20)$$

We assume

$$-\frac{\partial p}{\partial \xi} = \frac{1}{2}(e^{in\tau} + e^{-in\tau}),$$
$$F(\eta, \tau) = f(\eta)e^{in\tau} + g(\eta)e^{-in\tau},$$
$$\theta(\eta, \tau) = \theta_1(\eta)e^{in\tau} + \theta_2(\eta)e^{-in\tau}, \quad (21)$$

where $f(\eta)$, $g(\eta)$, $\theta_1(\eta)$ and $\theta_2(\eta)$ are unknown functions.

On the use of equation (21), equations (16) and (18) yield

$$\frac{d^2\theta_1}{d\eta^2} - (R + inPr)\theta_1 = 0, \quad (22)$$

$$\frac{d^2\theta_2}{d\eta^2} - (R - inPr)\theta_2 = 0, \quad (23)$$

$$\frac{d^2 f}{d\eta^2} + Gr\theta_1 + \frac{1}{2} = \left[in + 2iK^2 + \frac{M^2(1+im)}{1+m^2}\right]f, \quad (24)$$

$$\frac{d^2 g}{d\eta^2} + Gr\theta_2 + \frac{1}{2} = \left[-in + 2iK^2 + \frac{M^2(1+im)}{1+m^2}\right]g \quad (25)$$

with the boundary conditions

$$f = g = 0,\ \theta_1 = \theta_2 = \frac{1}{2} \ \text{ at } \ \eta = -1,$$
$$f = g = 0,\ \theta_1 = \theta_2 = 0 \ \text{ at } \ \eta = 1. \quad (26)$$

The solutions of the equations (22)-(25) with the boundary conditions (26) are

$$\theta_1(\eta) = \frac{\sinh r_1(1-\eta)}{2\sinh 2r_1}, \quad (27)$$

$$\theta_2(\eta) = \frac{\sinh r_2(1-\eta)}{2\sinh 2r_2}, \quad (28)$$

$$f(\eta) = \frac{1}{2}\left[\frac{1}{r_3}\left(1 - \frac{\cosh r_3\eta}{\cosh r_3}\right) + \frac{Gr}{(r_1^2 - r_3^2)}\left\{\frac{\sinh r_3(1-\eta)}{\sinh 2r_3} - \frac{\sinh r_3(1-\eta)}{\sinh 2r_3}\right\}\right], \quad (29)$$

$$g(\eta) = \frac{1}{2}\left[\frac{1}{r_4}\left(1 - \frac{\cosh r_4\eta}{\cosh r_4}\right) + \frac{Gr}{(r_2^2 - r_4^2)}\left\{\frac{\sinh r_4(1-\eta)}{\sinh 2r_4} - \frac{\sinh r_4(1-\eta)}{\sinh 2r_4}\right\}\right]. \quad (30)$$

Substituting equations (27)-(30) in equation (21), the temperature and velocity distributions become

$$\theta(\eta, \tau) = \frac{1}{2}\left[\frac{\sinh r_1(1-\eta)}{\sinh 2r_1}e^{in\tau} + \frac{\sinh r_2(1-\eta)}{\sinh 2r_2}e^{-in\tau}\right], \quad (31)$$

$$F(\eta, \tau) = \frac{1}{2}\left[\frac{1}{r_3}\left(1 - \frac{\cosh r_3\eta}{\cosh r_3}\right) + \frac{Gr}{(r_1^2 - r_3^2)}\left\{\frac{\sinh r_3(1-\eta)}{\sinh 2r_3} - \frac{\sinh r_3(1-\eta)}{\sinh 2r_3}\right\}\right]e^{in\tau}$$
$$+\frac{1}{2}\left[\frac{1}{r_4}\left(1 - \frac{\cosh r_4\eta}{\cosh r_4}\right) + \frac{Gr}{(r_2^2 - r_4^2)}\left\{\frac{\sinh r_4(1-\eta)}{\sinh 2r_4} - \frac{\sinh r_4(1-\eta)}{\sinh 2r_4}\right\}\right]e^{-in\tau}, \quad (32)$$

where

$$r_1, r_2 = (R \pm inPr)^{\frac{1}{2}},\ r_3, r_4 = \left[\frac{M^2}{1+m^2} \pm i\left(n + 2K^2 + \frac{mM^2}{1+m^2}\right)\right]^{\frac{1}{2}}. \quad (33)$$

On seperating into a real and imaginary parts, one can easily obtained from the equation (32) the velocity components u_1 and v_1.

3. RESULTS AND DISCUSSION

Here we have represented graphically the non-dimensional velocity components u_1 and v_1 and temperature distribution θ against η for several values of magnetic parameter M^2, radiation parameter R, Hall parameter m, rotation parameter K^2, Prandtl number Pr, Grashof number Gr, frequency parameter n and phase angle $n\tau$ in Figs.2-13. It is seen from Figs.2-4 that both the primary velocity u_1 and the magnitude of the secondary velocity v_1 decrease with an increase in either magnetic parameter M^2 or radiation parameter R or rotation parameter K^2. The application of the transverse magnetic field plays the important role of a resistive type force (Lorentz force) similar to drag force (that acts in the opposite direction of the fluid motion) which tends to resist the flow thereby reducing its velocity. There is a fall in velocity in the presence of radiation. It is revealed from Fig.5 that the primary velocity u_1 decreases while the magnitude of the secondary velocity v_1 increases with an increase in Hall parameter m. It is observed from Fig.6

that both the primary velocity u_1 and the magnitude of the secondary velocity v_1 increase with an increase in Prandtl number Pr. An increase in Grashof number leads to rise both the primary velocity u_1 and the magnitude of the secondary velocity v_1 shown in Fig.7. This is because, increase in Grashof number means more heating and less density. Fig.8 illustrates that both the primary velocity u_1 and the magnitude of the secondary velocity v_1 decrease with an increase in phase angle $n\tau$. It is seen from Fig.9 the primary velocity u_1 increases while the magnitude of the secondary velocity v_1 decreases with an increase in frequency parameter n. It is illustrated from Fig.10 that the fluid temperature θ decreases with an increase in radiation parameter R. This result qualitatively agrees with expectations, since the effect of radiation is to decrease the rate of energy transport to the fluid, thereby decreasing the temperature of the fluid. Fig.11 displays that the fluid temperature θ increases with an increase in Prandtl number Pr. This implies that an increase in Prandtl number leads to fall the thermal boundary layer flow. This is because fluids with large Pr have low thermal diffusivity which causes low heat penetration resulting in reduced thermal boundary layer. Fig.12 reveals that the fluid temperature θ decreases with an increase in phase angle $n\tau$. It is illustrated from Fig.13 that the fluid temperature θ increases near the plate at $(\eta = -1)$ and it decreases away from the plate at $(\eta = -1)$ with an increase in frequency parameter n.

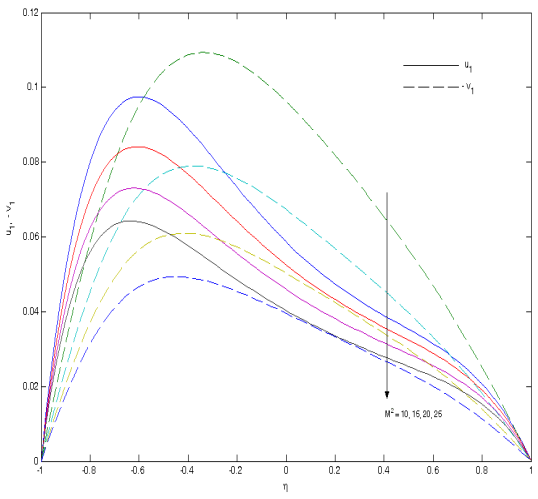

Figure 2: Velocity profiles for different M^2 when $R = 4$, $m = 0.5$, $Pr = 0.71$, $n = 1$, $K^2 = 3$, $Gr = 5$ and $n\tau = \frac{\pi}{4}$.

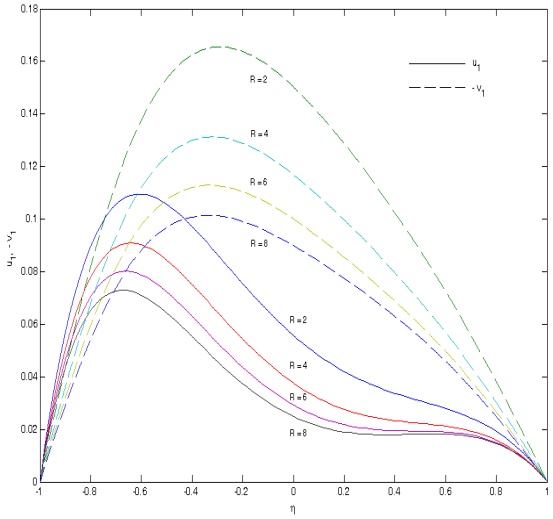

Figure 3: Velocity profiles for different R when $M^2 = 5$, $Gr = 5$, $n = 1$, $K^2 = 3$, $Pr = 0.71$, $m = 0.5$ and $n\tau = \frac{\pi}{4}$.

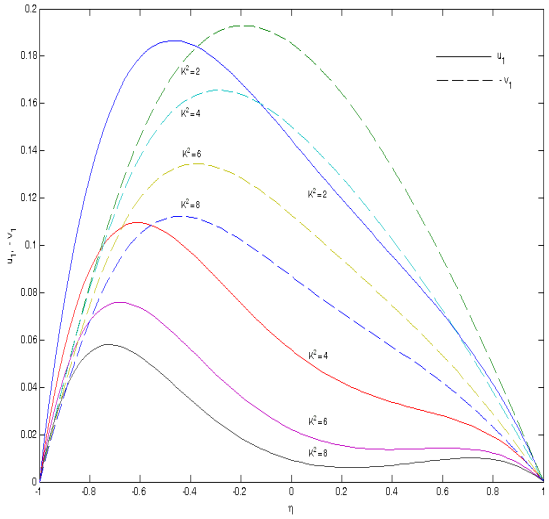

Figure 4: Velocity profiles for different K^2 when $M^2 = 5$, $R = 4$, $n = 1$, $m = 0.5$, $Gr = 5$, $Pr = 0.71$ and $n\tau = \frac{\pi}{4}$.

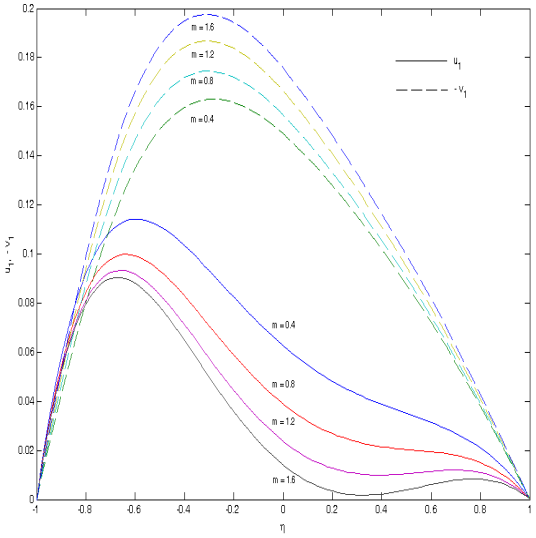

Figure 5: Velocity profiles for different m when $M^2 = 5$, $n = 1$, $K^2 = 3$, $R = 4$, $Gr = 5$, $Pr = 0.71$ and $n\tau = \frac{\pi}{4}$.

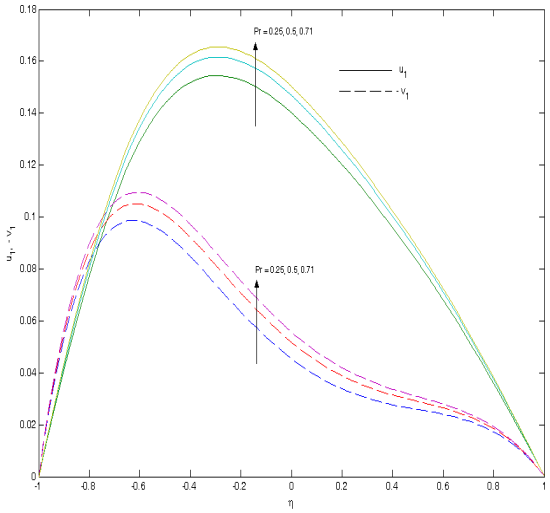

Figure 6: Velocity profiles for different Pr when $M^2 = 5$, $n = 1$, $K^2 = 3$, $R = 4$, $Gr = 5$, $m = 0.5$ and $n\tau = \frac{\pi}{4}$.

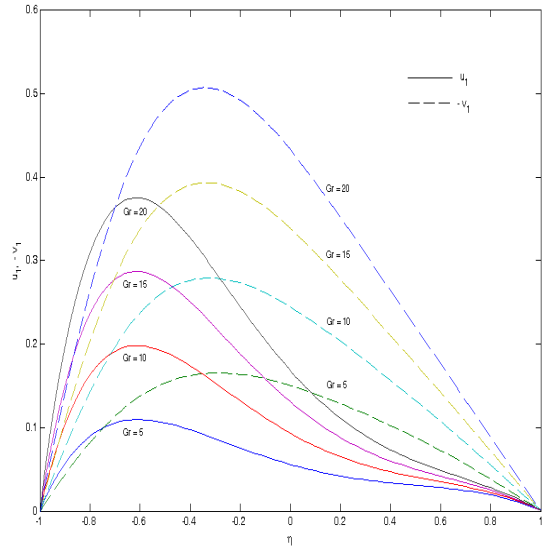

Figure 7: Velocity profiles for different Gr when $M^2 = 5$, $R = 4$, $n = 1$, $K^2 = 3$, $Pr = 0.71$, $m = 0.5$ and $n\tau = \frac{\pi}{4}$.

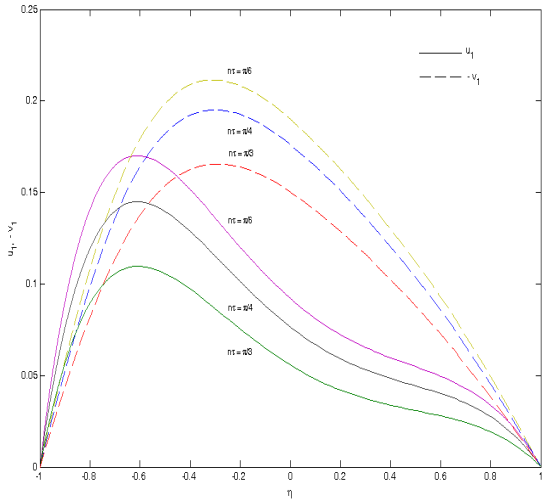

Figure 8: Velocity profiles for different $n\tau$ when $M^2 = 5$, $n = 1$, $K^2 = 3$, $R = 4$, $Gr = 5$, $m = 0.5$ and $Pr = 0.71$.

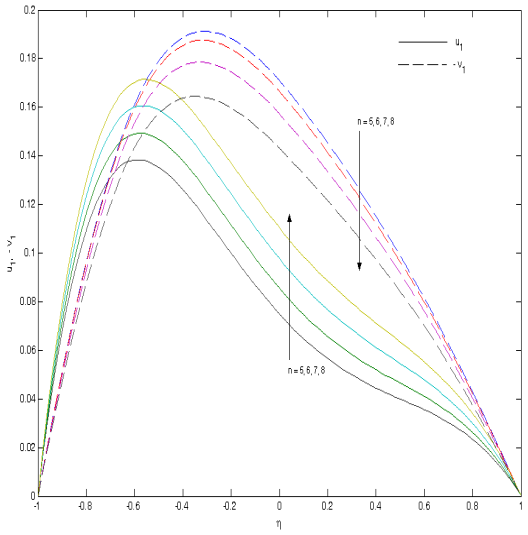

Figure 9: Velocity profiles for different n when $M^2 = 5$, $R = 4$, $K^2 = 3, Gr = 5$, $m = 0.5, Pr = 0.71$ and $n\tau = \frac{\pi}{4}$.

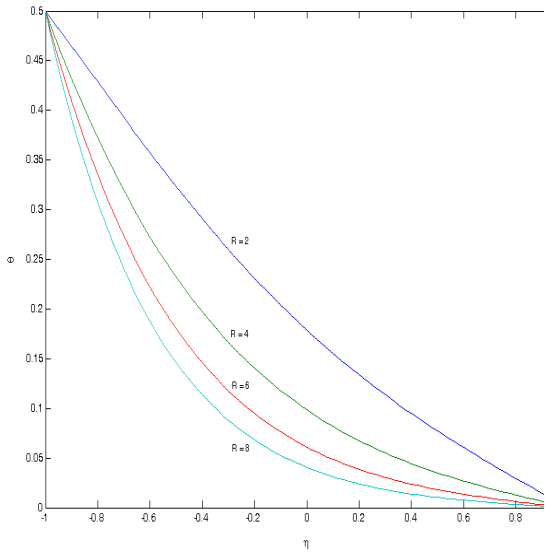

Figure 10: Temperature profiles for different R when $Pr = 0.71$, $n = 1$ and $n\tau = \frac{\pi}{4}$.

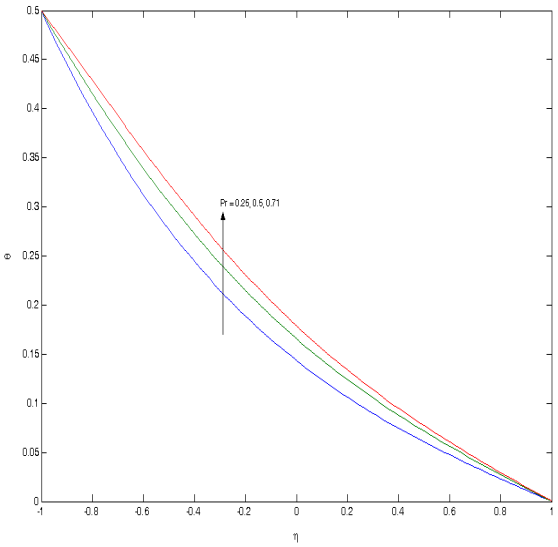

Figure 11: Temperature profiles for different Pr when $R = 4$, $n = 1$ and $n\tau = \frac{\pi}{4}$.

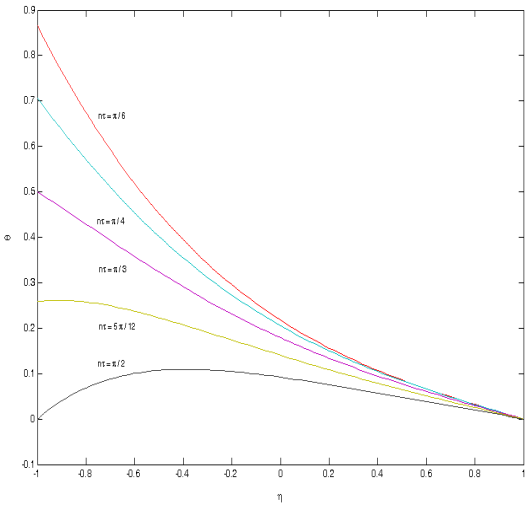

Figure 12: Temperature profiles for different $n\tau$ when $Pr = 0.71$, $n = 1$ and $R = 4$.

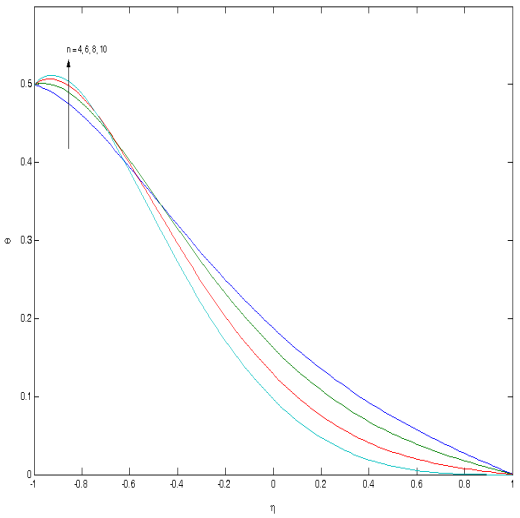

Figure 13: Temperature profiles for different n when $Pr = 0.71$, $R = 4$ and $n\tau = \frac{\pi}{4}$.

The rate of heat transfer at the plates $(\eta = \pm 1)$ are respectively given by

$$-\left(\frac{\partial\theta}{\partial\eta}\right)_{\eta=-1} = R_1\cos(n\tau+\phi_1), \tag{34}$$

$$-\left(\frac{\partial\theta}{\partial\eta}\right)_{\eta=1} = R_2\cos(n\tau+\phi_2), \tag{35}$$

where

$$R_1^2 = \frac{1}{(\cosh 4\alpha - \cos 4\beta)^2}\times$$
$$\times\left[(\alpha\sinh 4\alpha+\beta\sin 4\beta)^2+(\beta\sinh 4\alpha-\alpha\sin 4\beta)^2\right],$$
$$R_2^2 = \frac{4}{(\cosh 4\alpha-\cos 4\beta)^2}$$
$$\times\left[(\alpha\sinh 2\alpha\cos 2\beta+\beta\cosh 2\alpha\sin 2\beta)^2+\right.$$
$$\left.+(\beta\sinh 2\alpha\cos 2\beta-\alpha\cosh 2\alpha\sin 2\beta)^2\right]$$
$$\tan\phi_1 = \frac{\beta\sinh 4\alpha-\alpha\sin 4\beta}{\alpha\sinh 4\alpha+\beta\sin 4\beta}, \tag{36}$$
$$\tan\phi_2 = \frac{\beta\sinh 2\alpha\cos 2\beta-\alpha\cosh 2\alpha\sin 2\beta}{\alpha\sinh 2\alpha\cos 2\beta+\beta\cosh 2\alpha\sin 2\beta},$$
$$\alpha,\beta = \frac{1}{\sqrt{2}}\left[\left(R^2+n^2Pr^2\right)^{1/2}\pm R\right]^{1/2}.$$

Numerical results of the amplitude R_1 and the tangent of phase $\tan\phi_1$ of the rate of heat transfer $-\left(\frac{\partial\theta}{\partial\eta}\right)_{\eta=-1}$ at the plate $(\eta=-1)$ and the amplitude R_2 and the tangent of phase $\tan\phi_2$ of the rate of heat transfer $-\left(\frac{\partial\theta}{\partial\eta}\right)_{\eta=1}$ at the plate $(\eta=1)$ against the radiation parameter R are presented in the Tables 1- 4 for several values of radiation parameter R, Prandtl number Pr and frequency parameter n. Table 1 shows that the amplitude R_1 increases with an increase in either radiation parameter R or Prandtl number Pr or frequency parameter n. It is revealed from Table 2 that for fixed values of radiation parameter R, the tangent of phase $\tan\phi_1$ increases with an increase in either Prandtl number Pr or frequency parameter n. It is seen that for fixed values of Pr and n, the tangent of phase $\tan\phi_1$ decreases with an increase in radiation parameter R. Table 3 displays that the amplitude R_2 increases with an increase in either radiation parameter R or Prandtl number Pr or frequency parameter n. It is illustrated from Table 4 that for fixed values of radiation parameter R, the tangent of phase $\tan\phi_2$ increases with an increase in either Prandtl number Pr or frequency parameter n. Further, it is seen that for fixed values of Pr and n, the tangent of phase $\tan\phi_2$ decreases with an increase in radiation parameter R.

Table 1. Amplitude R_1 of the rate of heat transfer at the plate $(\eta = -1)$

	Pr				*n*			
R	0.25	0.5	0.71	1.5	2	3	4	5
2	2.89710	3.02958	3.18935	3.97862	3.18935	3.52095	3.89221	4.27952
4	4.01863	4.06514	4.12584	4.48793	4.12584	4.26647	4.44403	4.64707
6	4.90806	4.93339	4.96710	5.18241	4.96710	5.04793	5.15509	5.28399
8	5.66252	5.67900	5.70110	5.84651	5.70110	5.75485	5.82767	5.91750

Table 2. Tangent of phase $\tan\phi_1$ of the rate of heat transfer at the plate $(\eta = -1)$

	Pr				*n*			
R	0.25	0.5	0.71	1.5	2	3	4	5
2	0.11789	0.22445	0.30044	0.47932	0.30044	0.39949	0.46742	0.51270
4	0.06191	0.12236	0.17107	0.32947	0.17107	0.24753	0.31540	0.37441
6	0.04155	0.08266	0.11657	0.23559	0.11657	0.17197	0.22429	0.27302
8	0.03121	0.06224	0.08803	0.18125	0.08803	0.13080	0.17216	0.21180

Table 3. Amplitude R_2 of the rate of heat transfer at the plate $(\eta = 1)$

	Pr				*n*			
R	0.25	0.5	0.71	1.5	2	3	4	5
2	0.18725	0.23871	0.29837	0.59293	0.29837	0.42061	0.55991	0.70981
4	0.07751	0.08942	0.10423	0.18789	0.10423	0.13705	0.17777	0.22502
6	0.03793	0.04201	0.04721	0.07821	0.04721	0.05911	0.07435	0.09260
8	0.02034	0.02202	0.02420	0.03754	0.02420	0.02927	0.03586	0.04386

Table 4. Tangent of phase $\tan\phi_2$ of the rate of heat transfer at the plate $(\eta = 1)$

	Pr				*n*			
R	0.25	0.5	0.71	1.5	2	3	4	5
2	0.20762	0.31852	0.34382	0.27404	0.34382	0.32338	0.28306	0.24520
4	0.17963	0.31830	0.39137	0.42848	0.39137	0.44004	0.43374	0.40543
6	0.15827	0.29369	0.37986	0.49713	0.37986	0.46651	0.49592	0.49150
8	0.14288	0.27095	0.35951	0.52378	0.35951	0.46385	0.51731	0.53439

The non-dimensional shear stresses at the plates $\eta = \pm 1$ are

$$\left(\frac{\partial u_1}{\partial \eta}\right)_{\eta=-1} = R_3 \cos(n\tau + \phi_3), \tag{37}$$

$$\left(\frac{\partial v_1}{\partial \eta}\right)_{\eta=1} = R_4 \cos(n\tau + \phi_4), \tag{38}$$

where

$$R_3^2 = \left[\left(f_r'(-1) + g_r'(-1)\right)\right]^2 + \left[\left(f_i'(-1) - g_i'(-1)\right)\right]^2,$$

$$R_4^2 = \left[\left(f_r'(1) + g_r'(1)\right)\right]^2 + \left[\left(f_i'(1) - g_i'(1)\right)\right]^2,$$

$$\tan\phi_3 = \left[\frac{\left(f_i'(-1) - g_i'(-1)\right)}{\left(f_r'(-1) + g_r'(-1)\right)}\right], \tag{39}$$

$$\tan\phi_4 = \left[\frac{(f_i'(1)-g_i'(1))}{(f_r'(1)+g_r'(1))}\right],$$

$$f'(\eta) = -\frac{1}{2}\left[\frac{\sinh r_3\eta}{r_3\cosh r_3} + \right.$$
$$\left. + \frac{Gr}{(r_1^2-r_3^2)}\left\{r_3\frac{\cosh r_3(1-\eta)}{\sinh 2r_3} - r_1\frac{\cosh r_1(1-\eta)}{\sinh 2r_1}\right\}\right],$$

$$g'(\eta) = -\frac{1}{2}\left[\frac{\sinh r_4\eta}{r_4\cosh r_4} + \right.$$
$$\left. + \frac{Gr}{(r_2^2-r_4^2)}\left\{r_4\frac{\cosh r_4(1-\eta)}{\sinh 2r_4} - r_2\frac{\cosh r_2(1-\eta)}{\sinh 2r_2}\right\}\right]$$

and f_r', g_r', f_i', g_i' are respectively stand for real and imaginary parts of f' and g' and r_1, r_2, r_3 and r_4 are given by (33). Numerical results of the amplitude R_3 and the tangent of phase $\tan\phi_3$ of the shear stress at plate $(\eta = -1)$ due to the primary flow and the amplitude R_4 and the tangent of phase $\tan\phi_4$ of the shear stress at plate $(\eta = 1)$ due to the secondary flow are presented in Figs.14-21 against radiation parameter R for several values of magnetic parameter M^2, rotation parameter K^2, Prandtl number Pr and frequency parameter n when $n\tau = \frac{\pi}{4}$ and $Gr = 5$. Fig.14 illustrates that both the amplitudes R_3 and R_4 decrease with an increase in magnetic parameter M^2. It is seen from Fig.15 that both the magnitude of the tangent phases, $\tan\phi_3$ and $\tan\phi_4$ decrease with an increase in magnetic parameter M^2. Fig.16 reveals that the amplitudes R_3 increases whereas the amplitude R_4 decreases with an increase in Hall parameter m for fixed values of radiation parameter R. Fig.17 shows that for fixed values of radiation parameter R, the magnitude of the tangent phase $\tan\phi_3$ increases whereas the tangent of phase, $\tan\phi_4$ decreases with an increase in Hall parameter m. It is seen from Fig.18 that both the amplitudes R_3 and R_4 decrease with an increase in rotation parameter K^2. Fig.19 shows that the magnitude of the tangent phase, $\tan\phi_3$ increases whereas the tangent of phase, $\tan\phi_4$ decreases with an increase in rotation parameter K^2. It is seen from Fig.20 that both the amplitudes R_3 and R_4 increase with an increase in frequency parameter n. Fig.21 shows that the magnitude of the tangent phase, $\tan\phi_3$ increases whereas the tangent of phase, $\tan\phi_4$ decreases with an increase in frequency parameter n.

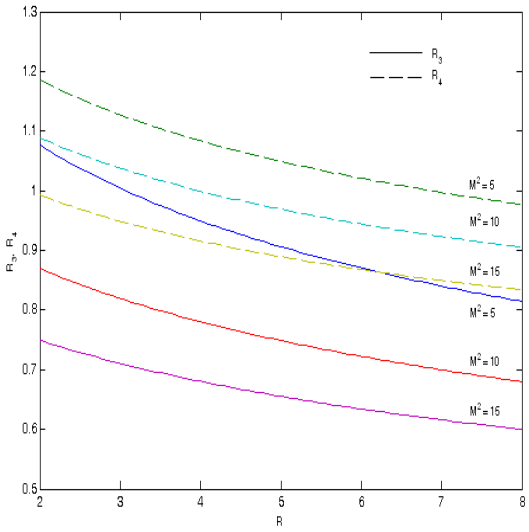

Figure 14: Variation of R_3 and R_4 for different M^2 when $m = 0.5$, $Pr = 0.71$ and $K^2 = 4$

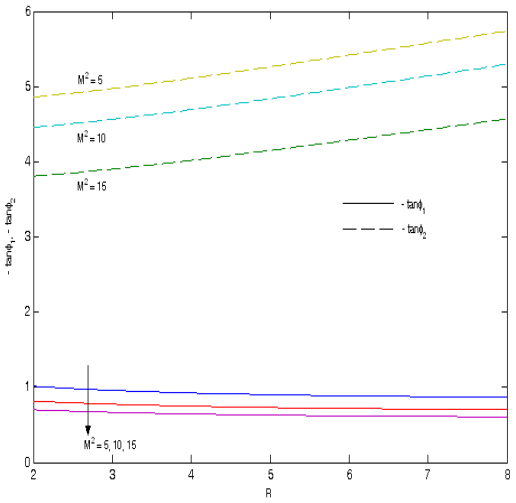

Figure 15: Variation of $\tan\phi_3$ and $\tan\phi_4$ for different M^2 when $Pr = 0.71$, $m = 0.5$ and $K^2 = 4$

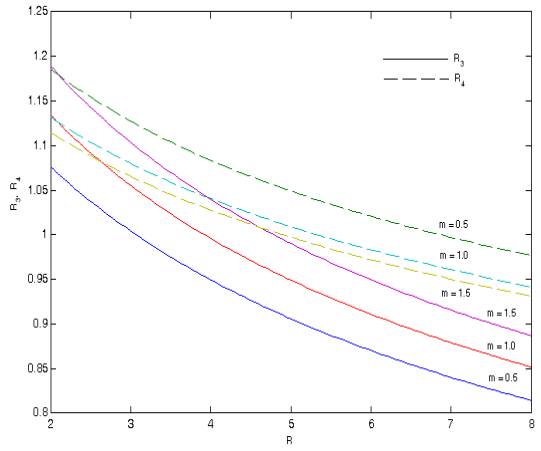

Figure 16: Variation of R_3 and R_4 for different m when $M^2 = 5$, $Pr = 0.71$ and $K^2 = 4$

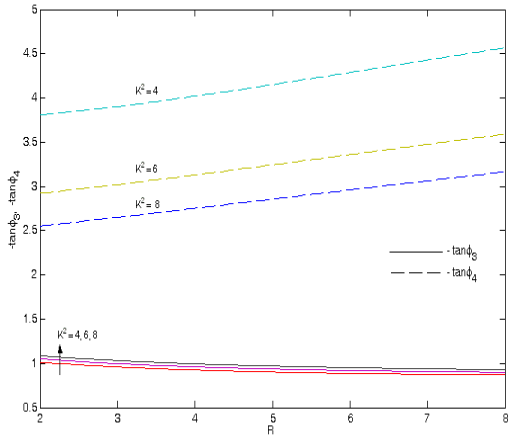

Figure 19: Variation of $\tan\phi_3$ and $\tan\phi_4$ for different K^2 when $M^2 = 5$, $Pr = 0.71$ and $m = 0.5$

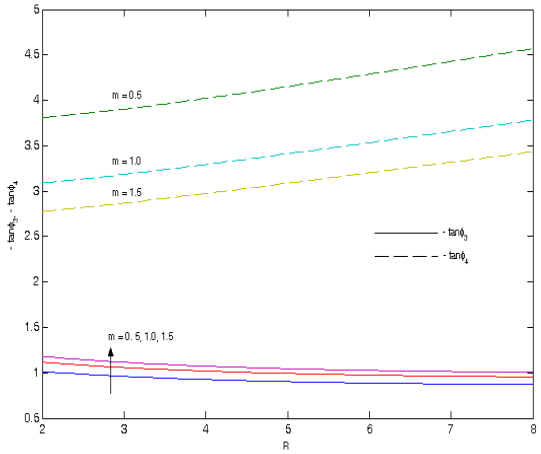

Figure 17: Variation of $\tan\phi_3$ and $\tan\phi_4$ for different m when $M^2 = 5$, $Pr = 0.71$ and $K^2 = 4$

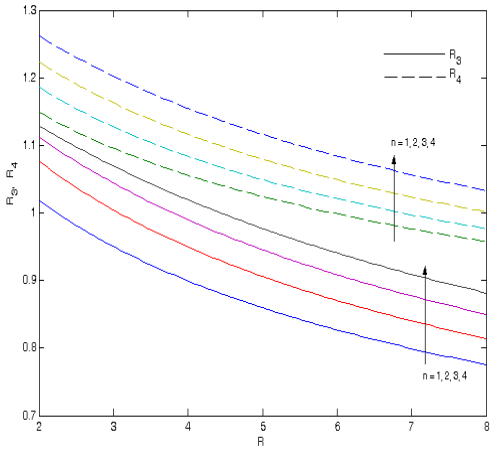

Figure 20: Variation of R_3 and R_4 for different n when $M^2 = 5$, $K^2 = 4$, $Pr = 0.71$ and $m = 0.5$

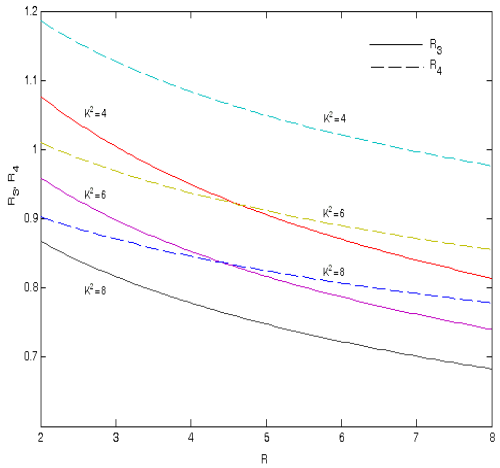

Figure 18: Variation of R_3 and R_4 for different K^2 when $M^2 = 5$, $Pr = 0.71$ and $m = 0.5$

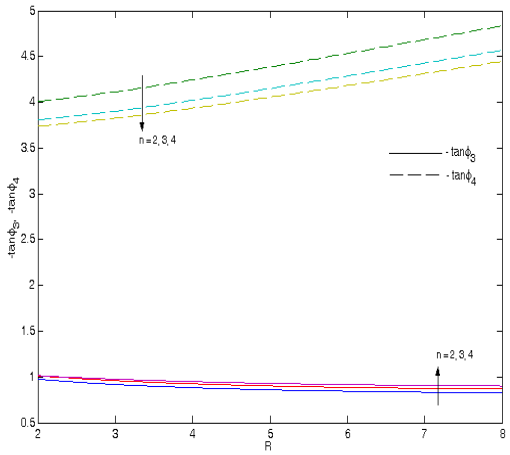

Figure 21: Variation of $\tan\phi_3$ and $\tan\phi_4$ for different n when $M^2 = 5$, $Pr = 0.71$ and $K^2 = 4$

4. CONCLUSION

The effects of Hall current and radiation on MHD mixed convection in a rotating vertical channel temperature in the presence of a uniform transverse magnetic field have been investigated. It is found that the Hall parameter m accelerates the primary velocity u_1 as well as the magnitude of the secondary velocity v_1. An increase in radiation parameter R leads to fall in the primary velocity u_1 as well as the magnitude of the secondary velocity v_1. Further, the amplitudes and tangent of phases of the shear stresses due to the primary and the secondary flows at the plates are significantly affected by characteristic parameters. The amplitudes and tangent of phases of the rate of heat transfer at the plates increases with an increase in radiation parameter R.

5. REFERENCES

[1] Helliwell, J. B. and Mosa, M.F. (1979). Radiative heat transfer in horizontal magnetohydrodynamic channel flow with buoyancy effects and an axial temperature gradient. *Int. J. Heat Mass Transfer*. 22: 657-668.

[2] Takhar, H.S. and Ram, P.C. (1991). Free convection in hydromagnetic flows of a viscous heat-generating fluid with wall temperature oscillation and Hall currents. *Astrophysics and Space Science*. 183: 193-198.

[3] Alagoa, K.D., Tay, G. and Abbey, T. M. (1998). Radiative and free convective effects of MHD flow through a porous medium between infinite parallel plates with time-dependent suction. *Astrophysics and Space Science*. 260(4): 455-468.

[4] Kinyanjui, M. Kwanza, J. K. and Uppal, S. M. (2001). Magnetohydrodynamic free convection heat and mass transfer of a heat generating fluid past an impulsively started infinite vertical porous plate with Hall current and radiation absorption. *Energy Conversion and Management*. 42(8): 917-931.

[5] Samad, M. A. and Rahman, M. M. (2006). Thermal radiation interaction with unsteady MHD flow past a vertical porous plate immersed in a porous medium. *J. Naval Architecture and Marine Engineering*. 3: 7-14.

[6] Chaudhary, R. C. and Jain, P.(2007). Hall effect on MHD mixed convection flow of a viscous elastic fluid past an infinite vertical porous plate with mass transfer and radiation. *UUR J. Phys*. 52(10): 110-127.

[7] Shit, G. C. and Haldar, R. Combined effects of thermal radiation and Hall current on MHD free convective flow and mass transfer over a stretching sheet with variable viscosity. *Physics Flu-dyn.* ar XIv: 1008.0165v1.

[8] Israel-Cookey, C., Amos, E. and Nwaigwe, C.(2010). MHD oscillatory Couette flow of a radiating viscous fluid in a porous medium with periodic wall temperature. *Ameri.J Sci. Indust. Res*. 1(2): 326-331.

[9] Ahmed, S. and Batin, A.(2010). Analytical model of MHD mixed convective radiating fluid with viscous dissipative heat. *Int. J. Engin. Sci. Tech.* 2(9): 4902-4911.

[10] Shateyi, S., Mosta, S. S. and Sibanda, P.(2010). The effects of thermal radiation, Hall currents, Soret and Dufour on MHD flow by mixed convection over a vertical surface in porous media. *Mathematical Problems in Engineering*.

[11] Singh, K. D. and Pathak, R.(2010). An analysis of an oscillatory rotating MHD Poiseuille flow with injection/suction and Hall currents. *Proc. Indian Natn. Sci. Acad.* 76: 201.

[12] Aurangzaib, Sharidan Shafie (2011). Effects of Soret and Dufour on unsteady MHD flow by mixed convection over a vertical surface in porous media with internal heat generation, chemical reaction and Hall current. *Canadian J. Sci. Engng. Math.* 2(4) : 153-162.

[13] Singh, K. D.(2012). Exact solution of MHD mixed convection periodic flow in a rotating vertical channel with heat radiation. *Int. J. Phys. Math. Sci.* 3(1): 14-30.

[14] Singh, K. D., Pathak, R. (2012). Effect of rotation and Hall current on mixed convection MHD flow through a porous medium in a vertical channel in presence of thermal radiation. *Indian J. Pure and Appl. Phys.* 50: 77-85.

[15] Cowling, T.G., Magnetohydrodynamics, Interscience Publisher, Inc, New York, 1957.

[16] Cogley, A. C. L., Vincenti, W. G., Gilles, E. S. (1968). Differential approximation for radiative heat transfer in a non grey gas near equilibrium. *Am. Inst. Aeronat. Astronaut. J*. 6:551-553.